10

Finding hydrogen leaks by means of the fiber Bragg gratings technology

Marc Debliquy [1], Driss Lahem [2], Christophe Caucheteur [1], Patrice Megret [1]
[1] *Université de Mons*
Belgium
[2] *Materia Nova*
Belgium

1. Introduction

Hydrogen participates to a wide range of chemical processes and it also appears during energy production and transport. It is widely used in aerospace applications where it acts as fuel for rockets. Nowadays, hydrogen is considered as an alternative source of energy for automotive applications and many developments are currently carried out on hydrogen fuel cells or engines. If these developments succeed economically, there will be an increased demand for hydrogen. With its high diffusivity, hydrogen is an extremely flammable gas. In air, it can burn at concentrations from about 4% with a flame velocity almost ten times higher than that of natural gas. Therefore, for security reasons, hydrogen leak detectors are highly important in industrial and practical applications.

In this frame, optical fiber sensors are particularly interesting in comparison with other technologies such as pellistors or semiconductor sensors (Yu&Yin, 2002). Indeed, optical fiber sensors offer unique advantages such as immunity to electromagnetic interference, light weight, flexibility, stability, high temperature tolerance, and even durability against high radiation environments. A single optical fiber can also offer distributed or quasi-distributed sensing, which is not possible with other sensing methods.

Among the different optical fiber sensor configurations, a great deal of the researches has been devoted to fiber Bragg gratings (FBGs) since they have been rapidly considered as excellent sensor elements, able to measure static and dynamic fields such as temperature, strain and pressure (Kersey et al. 1997; Othonos&Kalli, 1999). FBGs covered with Palladium have been widely investigated in the past for hydrogen detection (Sutapun et al., 1999; Tang et al., 1999; Peng et al. 1999; Maier, 2006). The sensing mechanism is based on the swelling of the Palladium coating, resulting in a stress on the grating. This sensor configuration suffers from a main drawback that is a quite long response time leading to a hysteresis effect between the responses obtained for increasing and decreasing hydrogen concentrations. Furthermore, the behaviour of such sensors in air environment is not known since all previous studies presented results of experiments conducted in nitrogen environment and mainly dedicated to aerospace applications.

We propose here a completely new hydrogen FBG-based sensor covered by a catalytic sensitive layer made of a ceramic doped with noble metal. In presence of hydrogen in air, an exothermic reaction occurs in the sensitive layer and leads to an increase of temperature measured by the FBG through a shift of its central wavelength. The obtained sensor response is linear and without hysteresis. The response is also selective and extremely fast for both increasing and decreasing hydrogen concentrations. The sensor has been tested in wet air and a very good sensitivity has been obtained whatever the relative humidity level of the environment.
The applications aimed are essentially hydrogen detection in air for the monitoring of storage places and pipe lines.

2. Generalities on Bragg gratings.

This paragraph summarizes the important concepts necessary to understand the principles of the presented hydrogen sensors.

2.1 Basic principle of fiber Bragg gratings

A fiber Bragg grating, called FBG, is a periodic and permanent modification of the core refractive index value along an optical fiber (Othonos & Kalli, 1999; Kashyap, 1999). This modification is generally obtained by exposing the core of a photosensitive optical fiber to an intense UV interference pattern. A fiber Bragg grating is defined by several physical parameters (figure 1). The grating length L is the optical fiber length along which the refractive index modulation is realized. The periodicity and the amplitude of the refractive index modulation are defined by Λ and δn, respectively.
The order of magnitude of these parameters typically varies from 0.2 µm to 100 µm for Λ, from a few mm to a few tens of cm for L and from 10^{-5} to 10^{-3} for δn. The inscription of such a perturbation in the fiber core induces light coupling between two counter-propagating modes. This mode coupling is produced for some wavelengths around the Bragg wavelength defined by the Bragg condition:

$$\lambda_{Bragg} = 2.n_{eff}.\Lambda \quad (1)$$

As shown on figure 1, a fiber Bragg grating acts as a selective mirror in wavelength around the Bragg wavelength for which there exists an energy transfer from the forward-going to the backward-going fundamental core mode. Physically, for each period of the fiber Bragg grating, a weak Fresnel reflection is produced due to a variation of the refractive index value. An important reflection is obtained when all the weak contributions add in phase. This condition is respected for the Bragg wavelength.
The grating planes are subject to temperature and strain perturbations, which modify the phase matching condition and lead to wavelength dependent reflectivity. Therefore tracking the wavelength at which the Bragg reflection occurs is the way to obtain the magnitude of the external perturbation.
For instance, the Bragg wavelength is influenced by the temperature or the stain applied to the fiber. One understands immediately the interest of these gratings to prepare temperature or strain sensors.

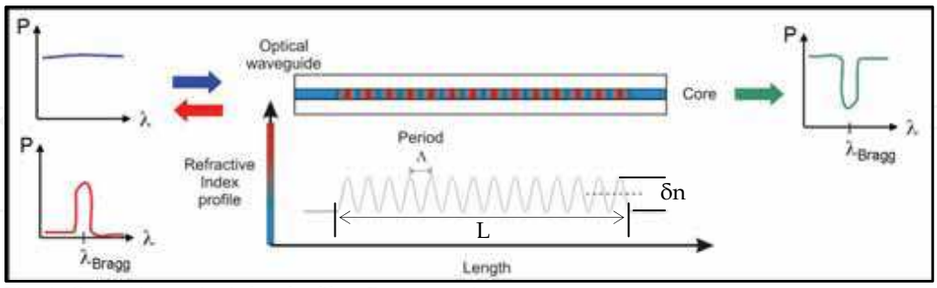

Fig. 1. Operating principle of a fiber Bragg grating.

A fiber Bragg grating is also able to couple light from a propagating mode to another mode characterized by a propagation constant that matches the spatial periodicity of the grating. This may result in coupling between the fundamental core mode and cladding or radiation modes. This coupling phenomenon is exploited in tilted fiber Bragg gratings.
It is also possible to manufacture fiber gratings that are transmissive so that they couple light between core and forward-going cladding modes. In this case the phase matching condition dictates a long grating periodicity of the order of several hundred microns. These components are known as long period fiber gratings LPFG.

2.2 Photosensitivity in optical fibers.

Photosensitivity of an optical fiber corresponds to its propensity to locally modify its core refractive index value when it is exposed to light with a wavelength and an intensity that depend on the core material.
Although photosensitivity is a very important property of an optical fiber, the complete mechanism responsible for this phenomenon is not yet fully understood. A lot of work is still in progress to better explain this phenomenon and to improve its knowledge. The study of the different mechanisms responsible for the optical fiber photosensitivity falls outside the scope of this document. This phenomenon was observed for a large number of fiber materials but is very important in germanium doped silica fibers. The photosensitivity is associated to the defects induced by germanium in the silica lattice. That is why these germanium doped fibers remain the most used for preparing Bragg gratings.
Pure silica SiO_2 is an amorphous material characterized by a tetrahedralstructure. Each oxygen atom links the silicon atoms of two adjacent structural molecules and is then shared by two tetrahedral units, as shown in figure 2(a). The combination of the different units forms a quasi-random structure (see figure 2 (b)).
The structure of germanium-doped silica is linked to that of pure silica since germanium, like silicon, is an element of the fourth group in the Mendeleev table of elements. A germanium atom can thus replace a silicon atom in the structure represented in figure 2.

Fig. 2. Tetrahedral structure of silica

The defects that are present in the structure are called color centers. Contrarily to silica that only exists in the form SiO_2, the two forms GeO and GeO_2 are stable and can be present in germanium-doped silica. The GeO defect, called germanium oxygen-deficient center (GODC), is often found in the structure of germanium-doped optical fiber. When it is present, the germanium or silicon atom is linked to only 3 oxygen atoms instead of 4 in the ideal structure and a bond is directly realized with a germanium atom (Ge-Si or Ge-Ge). This defect is characterized by an absorption band centered around 240 nm. The energy required to break the bond is around 5 eV.

There also exists a second type of structure of GODC. In this case, a germanium atom is bonded with only two oxygen atoms so that two electrons are free. This defect also presents an absorption peak at 240 nm. In their model, D.Hand and P. Russel link the mechanism of refractive index change to the photoinduced absorption change (Hand&Russel, 1990).This absorption creates new permanent defects that lead to a modification of the refractive index value. The modification of the absorption spectrum affects of course the refractive index since these values are linked by the Kramers-Kronig relationship (Russel&Hand, 1991).

It is in practice possible to obtain an important concentration of these two kinds of defects by reducing the quantity of oxygen during the fabrication process of the optical fiber.

There are substantial experimental evidences supporting the mechanism put forward by D. Hand and P. Russel in which the resultant color-centers are responsible for changes in the UV absorption spectrum of the glass and the refractive index change follows the Kramers-Kronig relationship. Many experiments support the GeE' defect center to be responsible for photosensitivity (Atkins et al., 1993;Tsai et al., 1993). However, the color center model cannot satisfactorily explain the behavior of all fiber types and the dopants used to modify the core refractive index. An alternative model based on glass densification induced by photoionization of the Ge defects has also found experimental support. This alternative model was proposed by M. Sceats and coworkers in 1993 (Sceats et al., 1993). The compaction/densification model is based on laser irradiation-induced density changes that result in refractive index changes. Irradiation by laser light at 248 nm has been shown to induce thermally reversible, linear compaction in amorphous silica, leading to refractive index changes. The model thus takes into account the presence of important stresses inside the optical fiber: mechanical, thermal stress coming from the optical fiber manufacturing process. These stresses can be relaxed by UV irradiation. The breaking of the bonds by UV irradiation (D. Hand and P. Russel mechanism) can also be responsible for the stress relaxing as this process causes a local density increase inside the optical fiber and a modification of the refractive index. Its exact contribution under various experimental conditions has still to be further investigated.

2.3 Techniques used to increase photosensitivity

Since the discovery of photosensitivity and its impact on the creation of fiber Bragg gratings, there has been considerable effort in understanding and increasing the photosensitivity in optical fibers. Standard single-mode optical fibers (3% germanium in the core) typically present index changes of about 3.10^{-5}. The addition of various co-dopants in germanosilicate optical fibers has resulted in photosensitivity enhancement. In particular, boron co-doping can lead to a saturated refractive index change about 4 times larger than that obtained in pure germanosilicate optical fibers. Sensitization techniques have also been developed for writing highly reflective gratings in germanosilicate optical fibers. An increase of the photoinduced refractive index modulation to values of the order of 10^{-3} and higher has been obtained via hydrogenation or flame brushing. These techniques consist in increasing the charge in hydrogen in the fiber core before grating inscription. For the hydrogenation (hydrogen loading) technique (Lemaire et al., 1993), optical fibers are placed in hydrogen gas environment at temperatures ranging from 20 °C to 75 °C and pressures from 20 atm to 750 atm, which results in diffusion of hydrogen molecules into the fiber core. Depending on the temperature and pressure values, the hydrogenation process can last from several hours to several days or even several weeks. During the UV irradiation, hydrogen allows the creation of GODC since it combines with oxygen atoms in order to form OH radicals. As hydrogen rapidly diffuses out of the optical fiber at ambient temperature, hydrogen-loaded optical fibers have to be maintained at low temperature prior to the fiber grating manufacturing process. Deuterium can also be used instead of hydrogen in order to avoid enhancement of the absorption peak of the OH bond around 1380 nm. This leads to the formation of OD radicals.

In the flame brushing technique (Bilodeau et al., 1993), the region of the optical fiber to be photosensitized is brushed repeatedly by a flame fueled with hydrogen and a small amount of oxygen, reaching a temperature of about 1700 °C. The photosensitization process takes approximately 20 minutes. At this very high temperature, hydrogen diffuses into the fiber core and reacts with the germanosilicate glass to produce GODC. This reaction creates a strong absorption band at 240 nm and leads to a highly photosensitive core. The flame brushing technique allows hydrogenation at ambient pressure but it can only be used locally as the flame is generally very small.

2.4 Temperature and mechanical strain sensitivities of uniform fiber Bragg gratings

The Bragg wavelength depends on the effective refractive index of the core and the spatial periodicity of the grating. These two parameters are affected by changes in strain and temperature. In particular, the effective refractive index is modified through the thermo-optic and strain-optic effect, respectively. Hence, from equation (1), the shift in the Bragg wavelength $\Delta\lambda_{Bragg}$ due to strain $\Delta\epsilon$ and temperature ΔT variations is given by:

$$\Delta\lambda_{Bragg} = 2\left(\Lambda\frac{dn_{eff}}{dT} + n_{eff}\frac{d\Lambda}{dT}\right)\Delta T + 2\left(\Lambda\frac{dn_{eff}}{d\epsilon} + n_{eff}\frac{d\Lambda}{d\epsilon}\right)\Delta\epsilon \quad (2)$$

The first term in Equation (2) represents the effect of temperature on the Bragg wavelength. The shift of the Bragg wavelength due to thermal expansion comes from the modification of the grating spacing and the refractive index. The relative wavelength shift due to a temperature change ΔT can be written as:

$$\frac{\Delta\lambda_{Bragg}}{\Delta T} = \lambda_{Bragg}\left(\frac{1}{n_{eff}}\frac{dn_{eff}}{dT} + \frac{1}{\Lambda}\frac{d\Lambda}{dT}\right) \quad (3)$$

where

$\frac{1}{n_{eff}}\frac{dn_{eff}}{dT}$ is the thermo-optic coefficient, which is approximately equal to 8.6 10^{-6} K^{-1} for germanium doped silica core optical fiber (Othonos & Kalli, 1999).

$\frac{1}{\Lambda}\frac{d\Lambda}{dT}$ is the thermal coefficient of the optical fiber, which is approximately equal to 0.55 10^{-6} K^{-1} for silica (Othonos & Kalli, 1999).

Clearly the refractive index change is the dominant effect. The order of magnitude of temperature sensitivity of the Bragg wavelength around 1550 nm is 10 pm/°C.

Figure 3 shows the experimental evolutions of the Bragg wavelength as a function of temperature for a 1 cm long uniform fiber Bragg grating. The grating was placed inside a thermal chamber regulated in temperature with an accuracy of the order of 0.1 °C.

The evolution is linear with a slope computed equal to 10.23 pm/°C.

Experiments were carried out for increasing and decreasing perturbations.

As shown in figure 3, no hysteresis was obtained, which is very important for sensing purposes.

The second term in equation (2) represents the effect of longitudinal strain on an optical fiber. It corresponds to a change in the grating periodicity and the strain-optic induced change in the refractive index. By defining the strain as $\in = \Delta\Lambda / \Lambda$, the change of the grating periodicity can be related to the applied strain since

$$\Lambda_s = \Lambda + \Delta\Lambda = \Lambda(1+\in) \tag{4}$$

where Λ_s represents the modified grating period after the application of the perturbation.

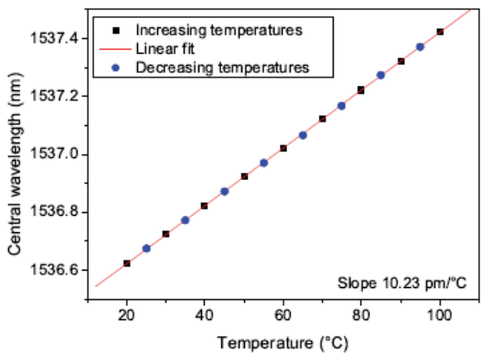

Fig. 3. Evolution of the peak wavelength as a function of temperature changes

The elasto-optic effect relates the refractive index change to the applied strain (Yarif, 1983):

$$\Delta n_{ij} = \Delta(\frac{1}{n_{eff}^2})ijj = \sum_{i=1}^{6}\sum_{j=1}^{6} p_{ij} \in_{ij} \tag{5}$$

where $\Delta\eta_{ij}$ is the change in the electric impermeability tensor, ε_j are the strain components and p_{ij} are the elements of the elasto-optic tensor. The form of the elasto-optic tensor, but not the magnitude of the coefficients p_{ij} can be derived from the symmetry of the material under

consideration. In its most general form, there are 36 different coefficients p_{ij} . For the class of isotropic materials, to which silica glass belongs, this number is reduced to two independent coefficients p_{11} and p_{12} (Yarif, 1983).
The magnitudes of the individual coefficients p_{ij} are dependent on the material considered. For pure bulk silica it was found that typical values measured at 628 nm are p_{11}=0.121 and p_{12}=0.270 (Bertholds & Dandliker, 1988). These values are often used when computing the influence of mechanical perturbations such as elongation and lateral compression of optical fibers. However due to the presence of doping elements in the core, the effective values for fibers may be different from those for bulk silica. Measurements on single-mode optical fibers at 628 nm yielded values of p_{11}=0.113 and p_{12}=0.252, respectively (Barlow, D. Payne, 1983). An error on these values of approximately 5% is possible because of the uncertainty on the value of the Poisson's ratio of the optical fiber.
Assuming that the grating is strained in the z direction only and that the fiber material follows Hooke's law, we obtain the shift of Bragg wavelength for an applied strain:

$$\Delta\lambda_{Bragg} = \lambda_{Bragg}(1 - p_e)\Delta\epsilon \tag{6}$$

$$p_e = \frac{n_{eff}^2}{2}[p_{12} - \nu(p_{11} + p_{12})] \tag{7}$$

where v is the Poisson's ratio.
Substitution of parameters (p_{11}=0.113, p_{12}=0.252, v=0.16 and n_{eff}=1.482) in equations (6) and (7) gives a strain-optic constant p_e= 0.21 and a sensitivity around 1550 nm of 1.2 pm/με.

2.5 Advantages of fiber Bragg grating sensors

The first fiber Bragg grating sensor was reported in 1989 by W. Morey and coworkers (Morey et al., 1989). The development of the external writing technique has considerably increased the interest in fiber Bragg grating sensors. This interest comes from the great potential that they have for a large number of sensing applications where are required measurements of strain and temperature (Morey et al., 1989), pressure (Xu et al., 1994), acceleration (Theriault et al., 1996), high magnetic field (Kersey & Marrone, 1994) and force (Bjerkan et al., 1996).
As already understood, fiber Bragg gratings are intrinsic optical sensors which modify the characteristic spectrum of an incident light signal since their physical parameters are affected by the external perturbation. The most widely used principle of operation of fiber Bragg grating sensors is to monitor the shift in wavelength of the reflected signal as a function of the external parameter to be measured.
The main advantage of fiber Bragg grating sensors is that the measurand information is wavelength-encoded. This property makes the sensor self-referencing and independent of fluctuating light levels. The system is therefore immune to source power and connector losses that affect many other types of optical fiber sensors. The very low insertion loss and narrowband wavelength reflection of fiber Bragg gratings offer convenient serial multiplexing along a single-mode optical fiber. There are further advantages of fiber Bragg gratings over conventional electrical strain gauges, such as linearity in response over many orders of magnitude. Many of them are intrinsic to the properties of optical fibers: immunity to electromagnetic interferences, light weight, flexibility, stability, high temperature tolerance and even durability in high radiation environments, which all contribute to obtain reproducible measurements. The small diameter of the optical fiber and the small length of fiber Bragg gratings make them compatible with applications for which slightly intrusive

probes are required, such as in the human body for temperature and/or chemical species profiling. Furthermore, fiber Bragg gratings can be easily embedded into materials to provide damage detection or internal strain field mapping. Fiber Bragg grating sensors are therefore very important components for the development of smart structure technology and for monitoring composite material curing and response. Nowadays such sensors offer real-time monitoring of civil structures and aerospace applications (Othonos & Kalli, 1999).

2.6 Long Period Fiber Gratings

We give here the basic theory of long period fiber gratings LPFG in order to have a fundamental understanding of the coupling mechanisms of such gratings in single mode optical fiber (Erdogan, 1997).

Let us note that long period fiber gratings are not Bragg gratings but they offer a lot of applications in sensing and will be used for chemical sensing purposes. The period of the refractive index modulation for a LPFG lies in the range 500 μm instead of 500 nm for a FBG. The operating principle of long period fiber gratings proposed by A. Vengsarkar and coworkers is illustrated in figure 4 (Vengsarkar et al., 1996). It can be seen that light vehiculated by the fundamental core mode is perturbed by the presence of the grating in the fiber core and is coupled to forward-going cladding modes. For long period fiber gratings, the difference between the propagation constant of the guided mode and the phase vector of the grating equals the propagation constant of one or more cladding modes at appropriate wavelengths.

Cladding modes result from the radiation modes that are trapped by the cladding-air interface. These modes attenuate rapidly due to bends in the fiber and absorption of cladding.

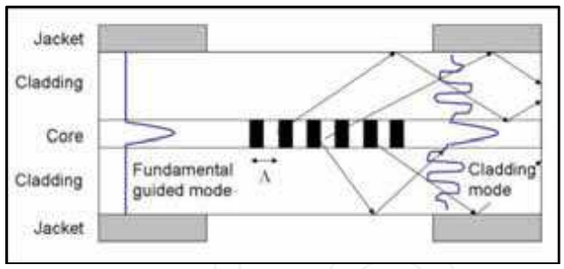

Fig. 4. Coupling of the fundamental guided mode to cladding modes in a long period fiber grating (not in scale)

Light at the phase-matched wavelengths is then lost from the fiber. For typical long period fiber gratings, more than one cladding mode can satisfy the phase-matching condition at different wavelengths and the guided mode can also be coupled to all those cladding modes. Typical transmitted spectra are thus composed of several cladding modes resonances. The important point is that these gratings can couple light out of the core. This has two consequences: energy can be given to the external medium and the transmission spectrum of the LPFG are very sensitive to refractive index changes of the external medium. These LPFG are therefore used to detect refractive index changes of the surrounding medium.

As in the case of uniform fiber Bragg gratings, LPFG's are sensitive to external parameters, in particular: temperature, strain or bending (James&Tatam, 2003). The sensitivity of long period fiber gratings characteristics to environmental parameters is influenced by the grating period (Bhatia, 1999) and by the optical fiber composition (Shima et al., 1997). However it is also influenced by the cladding modes to which coupling takes place. This combination of influences allows the design of long period fiber gratings that have a range of possible responses to a particular measurand beyond temperature and strain. A single long period fiber grating can indeed be characterized by attenuation bands that have a positive sensitivity to a measurand, others that are insensitive and others that have a negative sensitivity to the measurand. In summary, it is possible to finetune the sensitivity to temperature or strain by changing the geometry of the grating and the wavelength range.
The refractive index sensitivity of long period fiber gratings comes from the dependence of the phase matching condition on the effective refractive indices of the cladding modes. They are indeed function of the difference between the surrounding refractive index and the cladding refractive index. The central wavelengths of the attenuation bands are thus dependent on the surrounding refractive index, providing that the cladding has a higher refractive index than the surrounding medium.
The sensitivity to refractive index changes is spectrally manifested by central wavelength shifts and by changes in the minimum transmission value of the attenuation bands. The highest sensitivity is obtained for higher order modes and occurs for refractive index values close to that of the cladding (Patrick et al., 1998).
When the surrounding refractive index value matches that of the cladding, the cladding appears to be of infinite extent and a broadband radiation modes coupling with no distinct attenuation bands is obtained. When the surrounding refractive index is higher than that of the cladding, the central wavelengths of the attenuation bands present a considerably reduced sensitivity (Lee et al., 1997; Duhem et al., 1998).
A change in the form of the transmitted spectrum is however obtained since the peak to peak amplitudes of the attenuation resonances is reduced. In such a situation, the presence of attenuation bands is no longer due to the total internal reflection at the cladding/surrounding medium interface but comes from the Fresnel reflection that yields to attenuated cladding modes (Duhem et al., 1998).
The refractive index sensitivity has been exploited in a lot of applications such as chemical concentration sensing, liquid level sensing and even biosensing (James&Tatam, 2003).

3. Preparation of fiber gratings

This paragraph will shortly explain the most often used techniques to prepare fiber gratings eg to achieve the refraction index modulation in the core of the fiber thanks to the photosensitivity effect.
There are essentially 4 methods : interferometric method, phase mask, point to point and amplitude mask technique.

3.1 Interferometric method

For the interometric method (figure 5), also called transverse holographic technique (Meltz et al., 1989), one uses interferometer that splits the incoming UV laser light (at 244 nm) into two beams of equal intensity that were subsequently recombined in the core region of the

side exposed optical fiber to form an interference pattern, inducing a permanent refractive index modulation in the core. Furthermore, the periodicity of the refractive index modulation depends on the angle of recombination of the two beams. In each path of the free-space interferometer, a cylindrical lens focused the light onto the optical fiber.

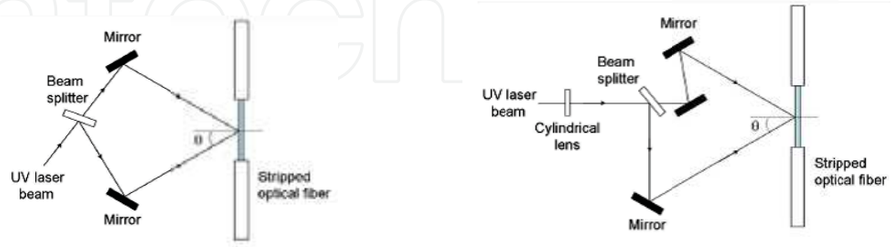

(a) (b)

Fig. 5. General amplitude-splitting interferometer (a) and improved version (b).

An improvement to the amplitude-splitting interferometer is shown in figure 5 (b). Indeed, in the first interferometer proposed by G. Meltz, the UV writing laser light is split into equal intensity beams that recombine after having undergone a different number of reflections in each optical path. Consequently the interfering beams acquire different polarization orientations, which results in a low-quality fringe pattern for laser beams having low spatial coherence. This problem is eliminated in the new implementation of the interferometer since it compensates for the beam splitter reflection by including a second mirror in one of the optical paths. The total number of reflections is the same in the two arms, which ensures that the two interfering beams are identical. A cylindrical lens is also used to focus the interfering beams to a fine line matching the fiber core. The resulting intensity obtained at the fiber core is higher and yields to an improvement of the grating fabrication.
The grating periodicity Λ, which is identical to the periodicity of the interference fringe pattern, depends on both the irradiation wavelength λ_{UV} and the half angle between the intersecting UV beams θ. The period of the grating is then given by the following relationship (8):

$$\Delta = \frac{\lambda_{UV}}{2 sin\theta} \tag{8}$$

One of the advantages of the holographic technique is its flexibility. Indeed, it is possible to inscribe gratings of different lengths and to modify the period through varying the angle ϑ. The main inconvenient is the instability towards vibrations and air movements. This method is difficult to use for mass production.

3.2 The phase mask technique

The phase mask technique is one of the most effective methods for inscribing fiber Bragg gratings in photosensitive optical fiber. This technique uses a diffractive optical element called phase mask to spatially modulate the UV writing beam. A phase mask is a relief grating realized in a pure fused silica plate. The significant features of the phase mask are the grooves realized into a UV-transmitting silica mask plate, with a carefully controlled mark-space ratio as well as etch depth. The profile of the periodic relief grating is chosen

such that when a UV beam is incident on the phase mask, the zero-order diffracted beam is suppressed to less than a few percent (typically less than 3%) of the transmitted power. This is done by action on the depth of the interference fringes. In addition, the diffracted plus and minus first orders are maximized with more than 35% of the transmitted power for each of these diffraction orders. A near-field interference pattern is then produced by the interference of the plus and minus first-order diffracted beams. The periodicity of the fringes is one half that of the phase mask. Hence, one given phase mask yields only one Bragg wavelength. The interference pattern photo-imprints a refractive index modulation in the fiber core that is placed in close proximity to the phase mask, as shown in figure 6.

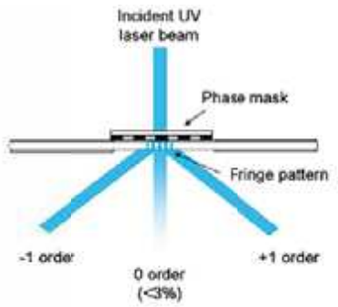

Fig. 6. Schematic of a phase mask used for fiber Bragg gratings inscription.

A cylindrical lens can also be used to focus the fringe pattern in the fiber core and to maximize the power density. The earliest experiments using the phase mask technique were performed by K.O. Hill and coworkers in 1993 (Hill et al., 1993). Since this original demonstration, the phase mask technique has been developed to a point where the inscription of nearly 100% reflective gratings is now routine with moderate UV optical power. Furthermore it is now possible to fabricate non uniform grating structures using the phase mask technique with specific phase masks.
The phase mask technique greatly reduces the complexity of the fiber grating fabrication system. The simplicity of using only one optical element provides a robust and stable method for the production of high quality fiber Bragg gratings. Since the optical fiber is placed directly behind the phase mask in the near field of the diffracting UV beams, stability problems due to mechanical vibrations are minimized. However, this technique is not flexible as the period of the gratings and the maximum length of the grating are fixed by the mask. Different masks are needed when the Bragg wavelength needs to be modified.

3.3 The point to point technique

The point to point technique is accomplished by inducing a change in the core refractive index corresponding to a grating plane one step at a time along the fiber core. This method is used to prepare long period gratings. This technique can also be applied to manufacture short period gratings when the spot is sufficiently focused (waist of the order of 0.25 µm) but it then requires a very stable and precise submicron translation system. In a typical experimental set-up, the UV laser beam passes through a slit before being focused on the core of an optical fiber, as shown in figure 7. As a result, the core refractive index in the

irradiated fiber section is changed locally. The fiber is then translated through a distance Λ corresponding to the grating period, in a direction parallel to the fiber axis. This process is repeated to form the grating structure in the fiber core. Depending on the grating length, the manufacturing process can be relatively long. Consequently, errors in the grating spacing due to thermal effects and/or small variations in the optical fiber strain can occur.

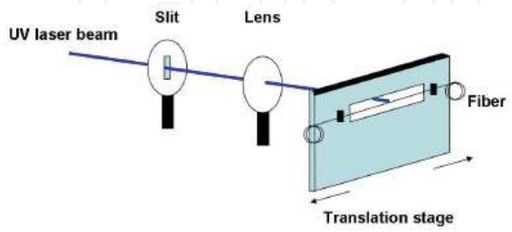

Fig. 7. Operating principle of the point to point technique.

3.4 Amplitude mask technique

The amplitude mask technique consists in placing a metal mask (generally in copper) in front of the optical fiber. The mask contains a pattern that is identically reproduced on the single mode optical fiber during the UV beam translation so that the periodicity of the obtained gratings is equivalent to that of the metal mask. To obtain a modification of the grating periodicity, it is thus required to use different metal masks.

4. Description of the hydrogen sensors

The different sensors consist in Uniform Fiber Bragg Gratings and/or Long Period Bragg Gratings covered with a sensitive layer that reacts with hydrogen (Caucheteur et al., 2008a). The sensitive layer consists in Platinum doped tungsten trioxide nano-lamellae.
The idea is to use the exothermic effect due to the combustion of H_2 on the surface of the sensitive coating which acts as a catalyst thanks to the following reactions (9 et 10):
The overall reaction is the combustion of hydrogen and WO_3 is not consumed.
The reaction heat of hydrogen combustion in normal conditions is 57.8 kcal/mol.

$$WO_3 + H_2 \leftrightarrow WO_2 + H_2O \quad (9)$$

$$WO_2 + ½O_2 \leftrightarrow WO_3 \quad (10)$$

4.1 Preparation of the Bragg gratings

Uniform FBGs and long period fiber gratings (LPFGs) were inscribed into standard single mode fiber by means of a frequency-doubled Argon-ion laser emitting at 244 nm. Prior to the UV exposure, the optical fiber was hydrogen-loaded at 70 °C and 200 atm during 48 hours. After the inscription, the gratings were annealed at 100 °C during 24 hours in order to stabilize their properties. Every grating was written in the middle of a 5 cm long stripped region of the optical fiber. The sensitive layer was deposited uniformly along the stripped region using the dip-coating technique, thus ensuring the same experimental conditions for all the gratings. As further explained, LPFGs were used for their radiative properties since

they are transmissive gratings that couple light from the fiber core to the cladding (James & Tatam, 2003).

4.2 Realization of the sensitive layer

Nano-sized tungsten oxide powder was prepared using sol-gel method (Okazaki et al., 2003; Caucheteur et al., 2008). To start, aqueous sol-gel of tungstic acid (H_2WO_4) was prepared from Na_2WO_4 with protonated cation-exchange resin. In a first stage, a gel consisting of $WO_3.H_2O$ was formed. The gel was washed, centrifuged several times with distilled water and dried in air at 60 °C for 6h. The powder consisting in nano-lamellae of tungsten oxide with high specific surface area (figure 8) is finally obtained. Appropriate amounts of hexachloroplatinic acid (H_2PtCl_6) solution were added to the obtained powder. The mixture was finally annealed at 500 °C for 1h in order to obtain WO_3 doped with Pt on its surface. At the end of the process, the active layer consists of WO_3 nano-lamellae (squares of about 1 µm x 1 µm x 50 nm) with Pt dispersed on their surface. The molar ratio Pt/W was about 1/14. After deposition on a substrate, a microporous structure is obtained with high specific area and high catalytic activity.

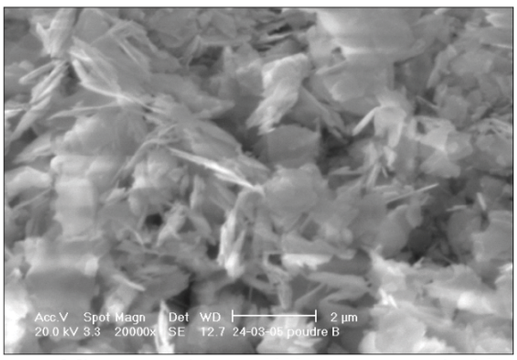

Fig. 8. Scanning Electron Microscopy image of the tungsten trioxide powder used in the sensitive layer. (Caucheteur et al., 2008 b)

4.3 Deposition of the sensitive layer on the fiber Bragg gratings

Prior to the deposition of the layer, the optical fiber was cleaned. The sensitive layer was then deposited, by using dip-coating technique, on the stripped optical fiber at a place where an FBG was written. The nanopowder of platinum doped tungsten oxide was mixed with a solvent (ethanol) so that the optical fiber could be immerged into the solution. Then the solvent evaporated at room temperature and the sensitive layer remained fixed on the optical fiber. The thickness of the deposited layer was measured of the order of 3 microns.

4. Experimental set-up

The set-up used to test the H_2 sensors in different air environments of various relative humidity levels is depicted in figure 9. A bubbler filled with distilled water is used to

control the relative humidity level of air between 0 and 90 %. Three mass flow controllers provided a mixture of air and hydrogen with variable H_2 concentrations from 0 to 4 % (the error on the determination of the H_2 concentration being equal to 0.05 %). The gas chamber was made of a 20 cm long and 1.5 cm wide glass cylinder with an inlet and an outlet to allow the gas mixtures flow through the chamber. Temperature and gas flow were continuously monitored. The amplitude spectrum of the tested gratings was measured by means of an ASE source covering the C+L bands (1520 - 1620 nm) and an optical spectrum analyzer (OSA) with an accuracy of 15 pm.

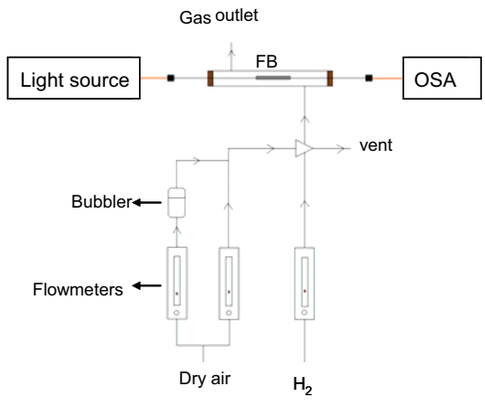

Fig. 9. Schematic of the experimental set-up used to test the H_2 fiber grating sensors.

5. Results

The response to hydrogen injections of sensors in different configurations was followed.
FBG of various lengths and hybrid LPFG+FBG structures were studied.
The effect of ambient temperature and relative humidity on the response were also checked for the different configurations.

5.1 Uniform Bragg gratings.

Figure 10 presents the results obtained on the transmitted spectrum of a 4 cm long FBG subjected to different H_2 concentrations in dry air at room temperature (20 °C). In presence of H_2 in air, a shift of the Bragg wavelength to the right appears due to the exothermic reaction that occurs between H_2 molecules and O_2 molecules inside the sensitive layer. The chemical reaction occurring in the sensitive layer is the oxidation of the H_2 molecules that generates H_2O molecules. For a 2 % concentration of H_2 in dry air, the measured wavelength shift is equal to 4 nm. It is equivalent to an increase of temperature around the FBG of about 400 °C since the temperature sensitivity of the FBG is of the order of 10 pm/°C.
It is important to mention that the exothermic reaction is initiated inside the sensitive layer when an energy threshold is reached. It is indeed required to bring sufficient energy so that the chemical reaction can be initiated. For the 4 cm long FBG tested above, the threshold in terms of H_2 concentration is equal to 1.0 % in dry air. That means that, for the first

measurement cycle realized for increasing H_2 concentrations, the grating did not react to H_2 concentrations below 1%. Then, once the chemical reaction has been initiated, it reacted to concentrations smaller than 1%, as shown on figure 4. Moreover, it was observed that the concentration threshold depended on the length of the grating. The threshold is bigger if the grating is shorter (figure 11). This is a very important feature of our sensor that limits its practical applications. That is why we have tried to quantify it as well as possible.

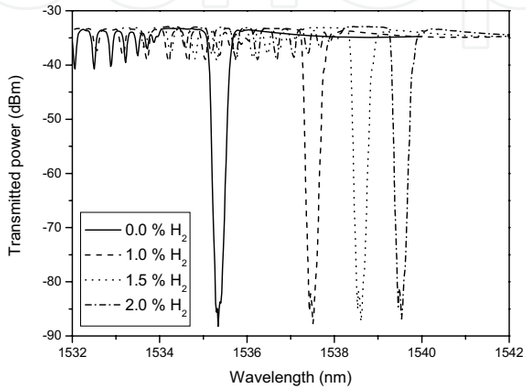

Fig. 10. Transmitted spectrum of a 4 cm long FBG in response to different H_2 concentrations in dry air at 20 °C.

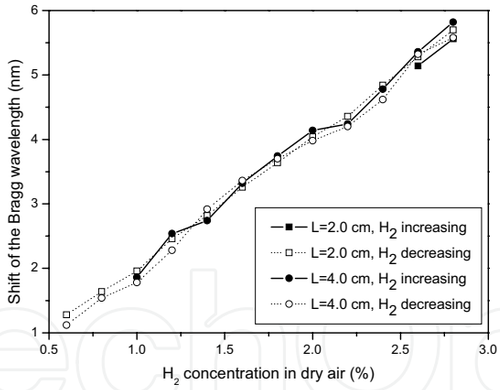

Fig. 11. Shift of the Bragg wavelength as function of the H_2 concentration in dry air at ambient temperature for different physical lengths of the gratings.

For that purpose, different strongly reflective uniform gratings characterized by different physical lengths were tested. The gratings were inscribed with the same velocity for the UV beam sweep along the phase mask and consequently, the longer gratings were more exposed to the UV interference pattern than the shorter gratings. The longest gratings (that are also the strongest in terms of coupling coefficient) were characterized by the presence of

important cladding modes resonances below the Bragg wavelength in the transmitted spectrum (approximately 3 dB of peak to peak amplitude for the low order cladding modes) as can be seen on figure 3, which demonstrates their strong coupling characteristics. Table 1 summarizes the results obtained in terms of detection threshold of H_2 concentrations for a set of 7 FBGs. The data were recorded for H_2 concentrations ranging from 0 to 3% and increasing by step of 0.1%.

Grating length (cm)	**Threshold (% H_2)**
0.5	No response up to 3%
1.0	~ 3.0
2.0	~ 2.5
2.5	~ 1.6
3.0	~ 1.4
3.5	~ 1.2
4.0	~ 1.0

Table 1. Thresholds for the detection of H_2 in dry air as function of the grating length during the first measurement cycle at room temperature.

These results reveal that the physical length of the inscribed grating influences the detection threshold of H_2 concentrations. Longer gratings allow for a reduction of the threshold. This comes from the fact that, as they are characterized by a strong coupling to both the backward going core mode and cladding modes, long gratings deliver some energy to the cladding that is finally collected by the sensitive layer and contributes to decrease the H_2 concentrations required to reach the threshold. This mechanism is possible since the refractive index modulation of the sensitive layer is higher than that of pure silica. Consequently, light that is outcoupled from the core of the fiber is guided into the sensitive layer and allows to initiate the chemical reaction between H_2 and O_2 molecules for small H_2 concentrations.

Figure 12 shows the wavelength shifts measured for all the tested gratings in response to increasing and decreasing H_2 concentrations. The plain curves were obtained for increasing H_2 concentrations (during the first measurement cycle) whereas the dotted curves were obtained for decreasing H_2 concentrations. The wavelength shifts were then converted to temperature variations around the tested FBGs (figure 13).

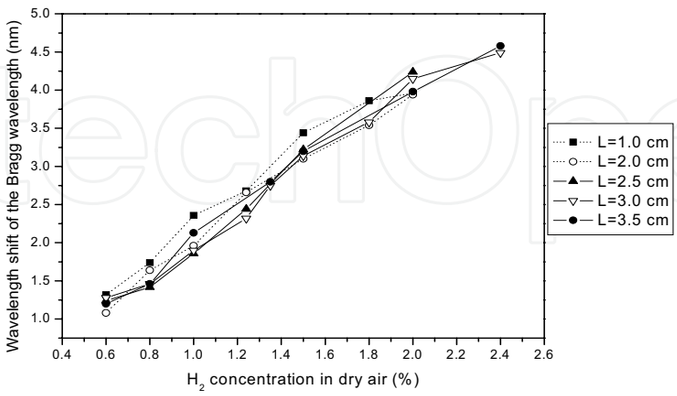

Fig. 12. Shift of the Bragg wavelength as function of the H_2 concentration in dry air at ambient temperature for different physical length of the gratings.

The results obtained from these experiments demonstrate that the grating length has no influence on the temperature delivered by the chemical reaction. The sensitivity of the sensor (the slope of the curve) is thus not dependent on the grating physical properties as expected since the reached temperature mainly depends on the hydrogen concentration.
Another important feature is the linear behaviour obtained in response to varying H_2 concentrations. Moreover, the data obtained for increasing H_2 concentrations match those obtained for decreasing H_2 concentrations so that there is no hysteresis in the sensor response. This characteristic is surely obtained owing to the very small response time (less than 4 seconds) of the sensor to varying H_2 concentrations.
The H_2-FBG sensors were also tested in wet air environments and the obtained results demonstrated that the threshold of detection of hydrogen concentration increases when the relative humidity level increases. For the 2.5 cm long FBG sensor , the threshold increased from 1.5 % to 3 % when the relative humidity level was changed from 0 % to 50 %. For the 4 cm long FBG, it increased from 1.0% to 1.5% when the relative humidity level was changed from 0 % to 90 %. This increase attributed to the presence of H_2O molecules adsorbed on the surface that tend to inhibit the reaction given in (9). The sensitivity to H_2 concentrations did not hange in wet air in comparison to that obtained in dry air because, as long as the threshold is passed, the temperature on the sensor is high enough to desorb the water molecules adsorbed on the surface and the reaction takes place as if water were not present. Indeed the temperature is higher than 100 °C when the reaction is ignited.
However, as shown on figure 14, the sensitivity in response to H_2 concentrations did not change in wet air in comparison to that obtained in dry air. The differences between the temperatures reached in dry air and in 50 % wet air all fell within ± 20 °C whatever the hydrogen concentration value.
Low temperature environments also led to an increase of the threshold value. At -30 °C, the detection threshold reached 1.8 % for the 4 cm long FBG. This value is still well below the 4 % explosion limit and it can be accepted in our applications.

The selectivity of the sensitive layer was tested with other gases such as carbon monoxide, methane and pure nitrogen. No answer was obtained, demonstrating that this sensor is specific to the detection of hydrogen in air.
These results can be rationalized by a simple model : the response of the sensor can be understood by examination of the heat flows exchanged on the sensitive layer surface in the presence of H_2.

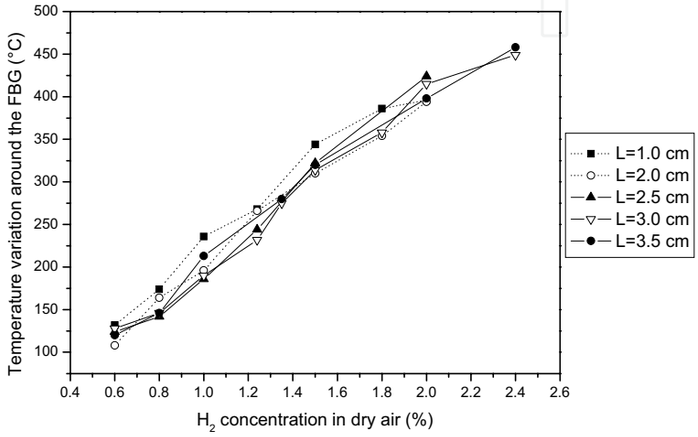

Fig. 13. Temperature variation around the FBG as function of the H_2 concentration in dry air at ambient temperature for different physical length of the gratings.

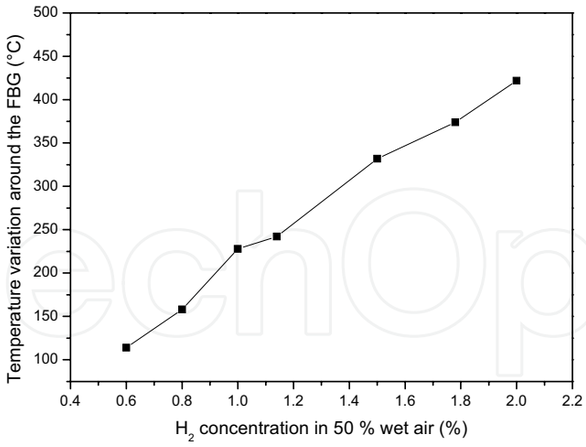

Fig. 14. Temperature variation around the 2.5 cm long FBG as function of the H_2 concentration in 50 % wet air at ambient temperature.

When the sensitive layer is in contact with a gas mixture of air and hydrogen, the oxidation of H_2 molecules by O_2 molecules contained in air occurs on its surface. This reaction is exothermic so that the temperature locally increases around the gratings. H_2 sensing is therefore based on the monitoring of the resonance wavelength shift induced by the temperature change. This reaction requires an activation energy equal to 0.15 eV (Appel et al., 2004). The temperature experienced by the grating results from the equilibrium between the heat flow delivered by the exothermic reaction $-\varphi_r$ and the heat flow lost by exchange with the surrounding medium φ_{th}. In a very good approximation, we may consider that φ_{th} is dominated by radiation so that it can be expressed by:

$$\varphi_{th} = \varepsilon\sigma(T^4 - T_e^4) \quad (11)$$

where ε is the emissivity of the WO_3 layer (close to 0.9 as it was estimated from infrared measurement of a surface of WO_3 heated to a known temperature), σ is the Stefan-Boltzmann constant (5.673 10-8 $W/(m^2.K^4)$), T is the absolute temperature measured by the grating and T_e is the absolute ambient temperature. φ_r is defined as :

$$\varphi_r = v.(-\Delta H_r) \quad (12)$$

$$v = k.C_{H2} \quad (13)$$

$$k = k_0.\exp(-\frac{Ea}{RT}) \quad (14)$$

where v is the reaction rate and $-\Delta H_r$ is the reaction heat and is equal to 57.8 kcal/mol. The reaction rate v is proportional to the concentration of hydrogen C_{H2} and depends on the temperature through the usual Arrhenius formula. E_a is the activation energy (0.15 eV), R is the gas constant equal to 8.31 J/(mol.K). k_0 depends on the amount of Pt per surface unit and reflects the sensitive layer efficiency. Its value is not precisely known in practice. Using Eq. (1) and (2), the sensor behavior can be semi-quantitatively simulated from the condition $\varphi_{th}=\varphi_r$ for different operating conditions. Figure 15 shows simulation results obtained for different ambient temperatures and for different sensitive layer efficiencies (the parameters put in the model were not optimized to exactly simulate the experimental results, reasonable values were used to qualitatively explain the observed results). Conformingly to our experiments, one can see on figure 15 that the detection threshold increases when both the ambient temperature and the sensitive layer efficiency decrease. Decreasing k_0 gives the same qualitative effect as a humidity level increase since water molecules tend to inhibit the exothermic reaction occurring on the sensitive layer. Hence, it may explain the increase of the threshold level. However, for the global evolution, as the temperature increases while hydrogen reacts, the adsorbed water molecules disappear from the surface and the occupied reaction sites are released and can participate to the reaction. Consequently, as soon as the temperature exceeds 60 °C, the effect of water almost vanishes and the equilibrium response remains the same as in absence of water.

Due to the activation energy (0.15 eV) of the chemical reaction, there exists a minimum of H_2 concentration below which the reaction will not start. In other words, there exists a threshold value in terms of H_2 concentration below which the sensor does not react. In practice, this threshold value can be decreased thanks to an external energy contribution. This could be done for instance by a local heating of the sensitive layer. One efficient way to do this is to exploit the light energy transported by the optical fiber. Indeed, at 1550 nm, the photon energy is about 0.7 eV and consequently, light that would be coupled from the core of the optical fiber towards the sensitive layer could favor the reaction for lower H_2

concentrations. This coupling mechanism is possible since the refractive index of the sensitive layer is slightly higher than that of pure silica. This explains the effect of the size of the grating. This effect was not simulated so far in our simple analysis.

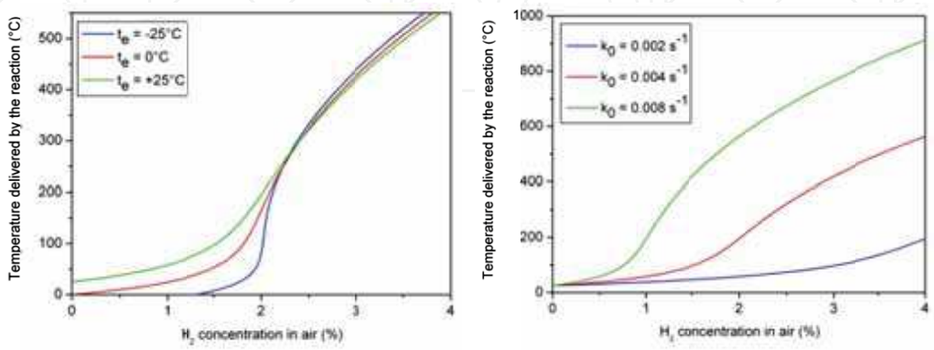

Fig. 15. Sensor responses simulated for different ambient temperatures (left – k_0=0.004 s^{-1}) and for different sensitive layer efficiencies (right – t_e=25°C).

5.2 Hybrid structure LPFG+FBG

In the previous paragraph, we have demonstrated the possibility to decrease the threshold value to 1 % in dry air with strongly reflective uniform FBGs. However, in that case, the FBGs are so strong that the accurate measurement of their Bragg wavelength is impossible (falls in the noise). Moreover, a drastic increase of the threshold was obtained in wet air and for temperatures below 0 °C, which strongly limits the use of uniform FBGs for H_2 sensing.

To avoid the limitations of uniform FBGs, a hybrid configuration consisting of the superimposition of a uniform FBG within an LPFG is presented. This solution takes profit of the light coupling to the cladding modes induced by the LPFG. Indeed, as the refractive index of the sensitive layer, consisting essentially in WO_3, is slightly higher than that of pure silica, the light outcoupled in the cladding penetrates the sensitive layer and its energy (photon energy around 1550 nm ~0.7 eV) favors the exothermic reaction.

The FBG is used as a probe to reflect the temperature change. The sensing mechanism is therefore based on the monitoring of the wavelength shift due to a temperature change in the reflected spectrum of the uniform FBG.

Both kinds of gratings were designed to minimize the detection threshold. The periodicity of the LPFG was chosen so as to obtain a strong resonance band (light coupled to the cladding) inside the spectral range of the optical source. A periodicity of 475 µm allowed us to obtain such a feature. A 1 cm long 545 nm period uniform FBG was then superimposed on the 3 cm long LPFG so as to obtain a point sensor. As shown in figure 16, it was written at the extremity of the LPFG to take a maximum profit of the light coupling provided by the LPFG. Figure 16 also shows the transmitted and reflected spectra of a typical hybrid configuration.

Our first experiments consisted in testing the behavior of hybrid configurations composed of 3 cm long LPFGs characterized by different refractive index modulations, yielding various transmission losses in the C+L bands. The LPFGs were inscribed with the same optical power (55 mW) but different exposure times (translation velocity of the UV beam

along the exposed fiber length set to 0.5 cm/s) so that the laser fluence was modified between the different inscriptions. In any case, the FBGs were characterized by a transmission loss of about 12 dB.

The radiating efficiency of every coated LPFG was evaluated by computing the ratio between the injected and transmitted optical powers integrated over the LPFG resonance bandwidth. The difference between these two quantities indeed reveals the total amount of radiated optical power. In addition, an examination of the fiber surface with an IR camera revealed that the radiation extends on a few centimeters beyond the LPFG end and is not uniform along the grating length. Hence, only a part of the total radiated power can be collected by the sensitive layer and is useful to favor the exothermic reaction. From our experiments, this part was roughly estimated to the third of the total radiated power. Figure 17 shows that the LPFG radiating efficiency increases with respect to the exposure time.

In particular, with the LPFG characterized by a 15 dB transmission loss, more than 60 % of the injected light is coupled out of the fiber core. For this grating and with the ASE source used here, we approximated to 0.2 mW the optical power collected by the sensitive layer. This quantity corresponds to about 1.5 10^{20} photons/(s.m^2), which is sufficient to favor the reaction with respect to the total number of H_2 adsorption sites per surface unit of the sensitive layer (estimated to 10^{19}/m^2 of fiber). The exact quantum efficiency is currently unknown and the involved mechanisms are thus being investigated.

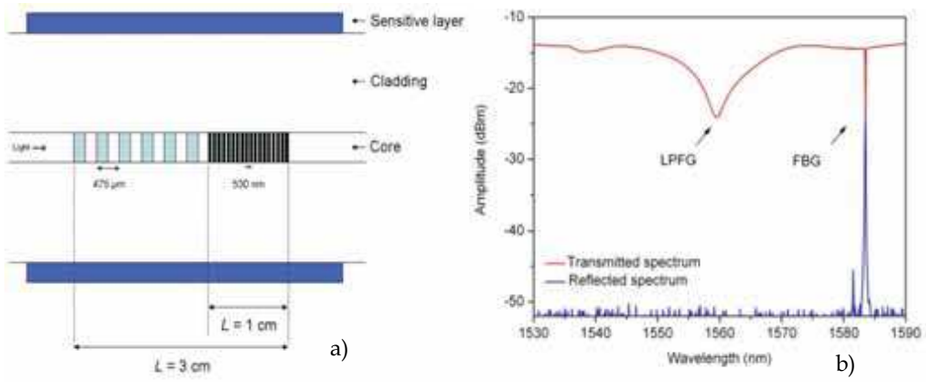

Fig. 16. Uniform FBG superimposed in a LPFG for H_2 detection (a) and transmitted/reflected spectra of this hybrid sensor on the C+L bands (b).

Figure 18 confirms the threshold reduction obtained provided by LPFGs. With the LPFG characterized by a 15 dB loss, the threshold has been measured equal to 0.6 % of H_2 concentration instead of 3 % with the equivalent single uniform FBG. It must be noticed that for all graphs, the response (wavelength shift versus concentration) is approximately the same, yielding the same sensitivity. This is due to the fact that the response is directly linked to the temperature reached thank to the exothermic reaction. For all sensors, the response is linear and reversible, with a mean sensitivity equal to 198 pm per 0.1 % of H_2 concentration, which is easy to detect with a standard instrumentation. The sensor response time was measured of about one second for H_2 concentrations above the detection threshold.

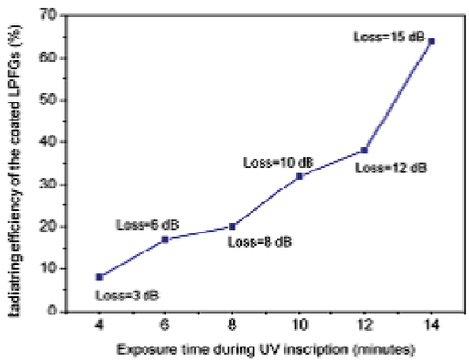

Fig. 17. Radiating efficiency as a function of the exposure time and corresponding LPFG transmission loss in the C+L bands.

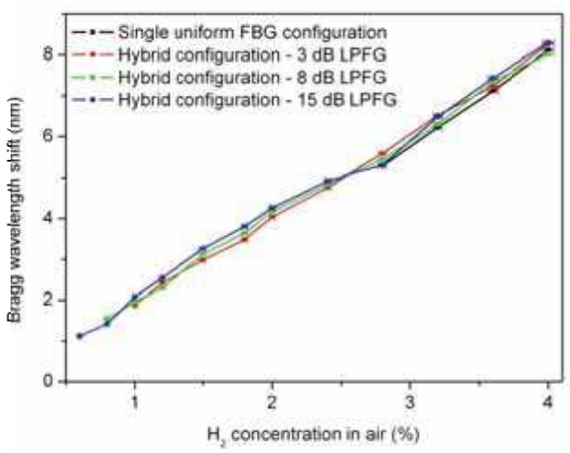

Fig. 18. Bragg wavelength shift as a function of the H_2 concentration in dry air for a single uniform FBG and hybrid gratings with various LPFGs.

The sensor behavior was also tested in wet air environments and at various temperatures. Figure 19 presents the Bragg wavelength shift of a hybrid sensor (configuration with the LPFG characterized by the 15 dB transmission loss) due to the H_2 concentration in different wet air environments. The H_2 detection threshold increases as the relative humidity level increases.

In 90 % wet air, the threshold has been measured equal to 0.9 % H_2 concentration. This is a clear improvement in comparison to a single 1 cm long uniform FBG sensor for which the threshold value has been measured higher than 3 % in 90 % wet air.

Finally, figure 20 confirms that a surrounding temperature decrease limits the sensor performances since more energy is required to initiate the exothermic reaction for a given H_2

concentration. However, while a single FBG is not sensitive to H_2 concentrations up to 4.0 % at -50 °C, the hybrid configuration presents a detection threshold equal to 1.5 %.

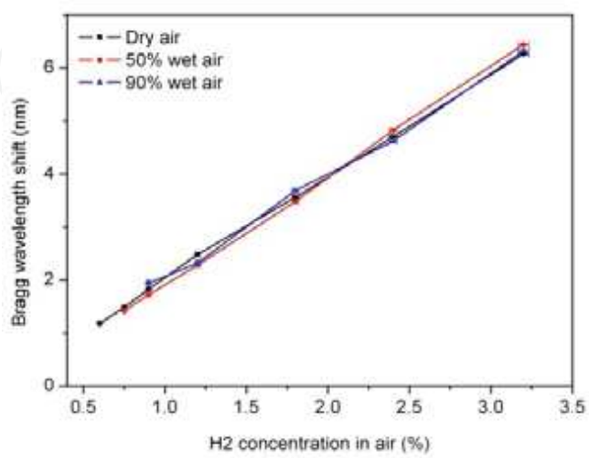

Fig. 19. Bragg wavelength shift as a function of the H_2 concentration in wet air for a hybrid sensor.

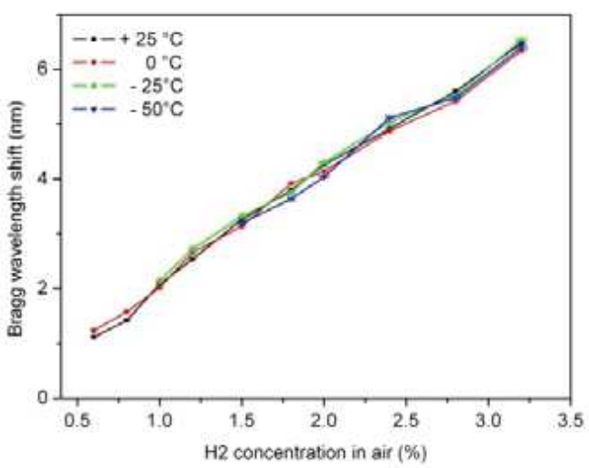

Fig. 20. Bragg wavelength shift as a function of the H_2 concentration at different temperatures.

Hence, in comparison to the use of single FBGs, the hybrid configuration presents the important advantage to decrease the detection threshold value for any experimental conditions. This feature is linked to the use of LPFGs and is possible without increasing the

optical source power density. It thus allows to work with a standard optical source (total power of 15 mW in our case), which keeps as low as possible the sensor price. Let us also mention that using uniform FBGs as probes instead of LPFGs presents two assets. First, the sensor response is encoded in the Bragg wavelength and is therefore not influenced by bending effects, which is not the case for LPFGs. Second, while the resonance band of an LPFG extends on several tens of nanometers (complicating the realization of quasi-distributed sensors with such gratings), a wavelength window of several nanometers is sufficient to record the reflected spectrum evolution of uniform FBGs. Consequently, thanks to the presence of uniform FBGs, the hybrid configuration can be used in frequency multiplexed systems. In particular, with LPFGs characterized by a transmission loss of 3 dB, up to 15 hybrid sensors can be cascaded along an optical fiber in the range of the used ASE source.

6. Conclusions and future work

In this chapter, a novel sensor is presented that is able to measure hydrogen leaks in air by means of optical fibers. The sensor is composed of a fiber Bragg grating covered by a catalytic sensitive layer. In presence of hydrogen in air, an exothermic reaction between H_2 molecules and O_2 molecules takes place on the sensitive layer, leading to an increase of temperature around the Bragg grating. The detection of H_2 concentrations is thus based on the monitoring of the Bragg wavelength shift in response to temperature changes.

Our sensor offers a very good sensitivity and a very fast response. It is selective to hydrogen and presents a rapid, linear response without hysteresis, which constitute very important sensor characteristics. It is also compatible with frequency multiplexing and can consequently allow for the realization of quasi-distributed sensors.

However, in its basic configuration, this sensor suffers from the presence of a detection threshold that limits the range of H_2 concentrations that it can detect. The possibility to decrease this threshold by working with highly reflective gratings has been shown.

The most elegant solution consists in superimposed hybrid fiber gratings coated with a catalytic sensitive layer that heats the gratings in the presence of hydrogen in air. In this hybrid configuration, the LPFG provided a light energy coupling to the sensitive layer to decrease the H_2 detection threshold while the FBG was used to track the temperature increase. Very good sensing performances have been reported: fast response, high sensitivity, reversibility, frequency multiplexing capability and H_2 concentrations detection well below the explosion limit of 4 %, whatever the relative humidity level and for temperatures down to -50 °C.

These hybrid configurations will be further studied in order to minimize the reaction threshold. Future work on these sensors would be to get full understanding and modeling of the sensor and then optimization of the sensor in order to minimize the detection limit imposed by the reaction threshold.

7. References

Appel C., Mantzaras J., Schaeren R., Bombach R. and Inaen A., "Catalytic combustion of hydrogen-air mixtures over platine: validation of hetero/homogeneous chemical reaction schemes," *Clean Air* **5**, 21-44 (2004).

Atkins R., Mizrahi V., Erdogan T. (1993), "248-nm induced vacuum UV spectral changes in optical fiber preform cores: Support for a colour centre model of photosensitivity" , *Electronics Letters*, vol. 29, num. 22, pp. 385–387, 1993.

Barlow A., Payne D. (1983), "The stress-optic effect in optical fibers" , *Journal of Quantum Electronics*, vol. 19, num. 5, pp. 834–839, 1983.

Bhatia V. (1999), "Applications of long-period gratings to single and multiparameter sensing" , Optics Express, vol. 4, pp. 457–466, 1999.

Bertholds A., Dandliker R. (1988), *J. of Lightwave Technology*, vol. 6, num. 1, pp. 17–20, 1988.

Bilodeau F., Malo B., Albert J., Johnson D., Hill K., Hibino Y., Abe M., Kawachi M.(1993), "Photosensitization of optical fiber and silica-on-silicon/silica waveguides" , *Optics Letters*, vol. 18, num. 12, pp. 953–955, 1993.

Bjerkan L., Hjelme D., Johannessen K. (1996), "Bragg grating sensor demodulation scheme using a semiconductor laser for measuring slamming forces of marine vehicle modes" , *Proceedings of the 11th International Conference on Optical Fiber Sensors*, pp. 236–239, 1996.

Caucheteur C., Debliquy M., Lahem D., Mégret P. (2008), 'Hydrogen leak optical sensor using radiating fiber gratings', *proceedings IEEE Sensors Conference*, Lecce, Italy, 27/10-29/10, 2008 (2008/08/27) pp 1281-1285. a)

Caucheteur C., Debliquy M., Lahem D. and Mégret P. (2008), "Catalytic fiber Bragg grating sensor for hydrogen leak detection in air," *IEEE Photon. Technol. Lett.* **20**, 96-98 (2008). b)

Duhem O., Henninot J.-F., Warenghem M., Douay M. (1998), "Demonstration of long-period grating efficient couplings with an external medium of a refractive index higher than that of silica" , *Applied Optics*, vol. 37, pp. 7223–7228, 1998.

Erdogan T. (1997), "Cladding-mode resonances in short- and long-period fiber grating filters", *Journal of the Optical Society of America A*, vol. 14, num. 8, pp. 1760–1773, 1997.

Hand D., Russel P.(1990) ,"Photoinduced refractive-index changes in germanosilicate fibers" , *Optics Letters*, vol. 15, num. 2, pp. 102–104, 1990.

Hill K., Malo B., Bilodeau F., Johnson D., Albert J. (1993), "Bragg gratings fabricated in monomode photosensitive optical fiber by UV exposure through a phase mask", *Applied Physics Letters*, vol. 62, pp. 1035–1037, 1993.

James S., Tatam R. (2003), "Optical fiber long-period grating sensors: characteristics and application" , *Measurement Science and Technology*, vol. 14,pp. R49–R61, 2003.

Kashyap R., Fiber Bragg gratings, Academic Press, 1999.

Kersey A., Marrone M. (1994), "Fiber Bragg high-magnetic-field probe" , *Proceedings of the 10th International Conference on Optical Fiber Sensors*, pp. 53–56, 1994.

Kersey A.D., Davis M.A., Patrick H.J., LeBlanc M., Koo K.P., Askins C.G., Putnam M.A., Friebele E. J.(1997) "Fiber Bragg grating sensors", *IEEE Journal of Lightwave Technology* **15**, pp 1442-1463, 1997.

Lee B., Liu Y., Lee S., Choi S., Jang J. (1997), "Displacements of the resonant peaks of a long-period fiber grating induced by a change of ambient refractive index", *Optics Letters*, Vol. 2, pp. 1769–1771, 1997.

Lemaire P., Atkins R., Mizrahi V., Reed W.(1993), "High pressure H2 loading as a technique for achieving ultrahigh UV photosensitivity and thermal sensitivity in GeO2 doped optical fibers" , *Electronics Letters*,vol. 29, pp. 1191–1193, 1993.

Meltz G., Morey W., Glenn W. (1989), "Formation of Bragg gratings in optical fibers by a transverse holographic method" , Optics Letters, vol. 14, num. 15, pp. 823–825, 1989.

Morey W., Meltz G., Glenn W.(1989), "Fiber optic Bragg grating sensors" , *Proceedings of SPIE*, pp. 98–107, 1989.

Othonos A., Kalli K.(1999) "*Fiber Bragg gratings: Fundamentals and applications in telecommunications and sensing",* Artech House, Norwood, MA, 1999.

Okazaki S., Nakagawa H., Asakura S., Tomiuchi Y., Tsuji N., Murayama H., Yashiya M. (2003), "Sensing characteristics of an optical fiber sensor for hydrogen leak", *Sensors and Actuators B* **93,** pp 142–147, 2003.

Patrick H., Chang C., Vohra S. (1997), "Long period fiber gratings for structural bend sensing", *Electronics Letters*, vol. 33, pp. 1893–1894, 1997.

Patrick H., Kersey A., Bucholtz F. (1998), "Analysis of the response of long period fiber gratings to external index of refraction" , *Journal of Lightwave Technology*, vol. 16, pp. 1606–1642, 1998.

Russel P., Hand D. (1991),"Optically-induced creation, transformation and organisation of defects and colour-centres in optical fibers", *Proceedings of the SPIE International Workshop on Photoinduced Self-Organization Effects in Optical Fiber*, pp. 47–54, Quebec City, Canada, 1991.

Sceats M., Atkins G., Poole S. (1993), "Photo-induced index changes in optical fibers", *Annual Reviews in Material Science*, vol. 23, pp. 381–410, 1993.

Shima K., Himeno K., Sakai T., Okude S., Wada A. (1997), "A novel temperature-insensitive long-period grating using boron-codoped germanosilicate core-fiber", *Proceedings of the International Conference on Optical Fiber Communications*, pp. 347–348, 1997.

Theriault S., Hill K., Bilodeau F., Johnson D., Albert J. (1996), "High-g accelerometer based on an in-fiber Bragg grating sensor" , *Proceedings of the 11th International Conference on Optical Fiber Sensors*, pp. 196–199, 1996.

Tsai T., Friebele E., Griscom D. (1993), "Thermal stability of photoinduced gratings and paramagnetic centers in Ge- and Ge/P-doped silica optical fibers" , *Optics Letters*, vol. 18, num. 12, pp. 935–937, 1993.

Vengsarkar A., Lemaire P., Judkins J., Bhatia V., Erdogan T., Sipe J. (1996), "Long-period fiber gratings as band-rejection filters" , *Journal of Ligthwave Technology*, vol. 14, num. 1, pp. 58–65, 1996.

Xu M., Geiger H., Dakin J.(1994), "Optical in-fiber grating high pressure sensor" , *Electronics Letters*, vol. 29, pp. 398–399, 1994.

Yariv A., Yeh P.(1983), *Optical waves in crystals: propagation and control of laser radiation*, *John* Wiley and Sons, 1983.

Yu F.T.S, Yin S, Yu Y.T.S. (2002), *Fiber Optic Sensors*, Marcel Dekker Inc., USA, 2002.

Optical Fiber New Developments

Edited by Christophe Lethien

ISBN 978-953-7619-50-3
Hard cover, 586 pages
Publisher InTech
Published online 01, December, 2009
Published in print edition December, 2009

The optical fibre technology is one of the hop topics developed in the beginning of the 21th century and could substantially benefit applications dealing with lighting, sensing and communication systems. Many improvements have been made in the past years to reduce the fibre attenuation and to improve the fibre performance. Nowadays, new applications have been developed over the scientific community and this book fits this paradigm. It summarizes the current status of know-how in optical fibre applications and represents a further source of information dealing with two main topics: the development of fibre optics sensors, and the application of optical fibre for telecommunication systems.

How to reference

In order to correctly reference this scholarly work, feel free to copy and paste the following:

Marc Debliquy, Driss Lahem, Christophe Caucheteur and Patrice Megret (2009). Finding Hydrogen Leaks by Means of the Fiber Bragg Gratings Technology, Optical Fiber New Developments, Christophe Lethien (Ed.), ISBN: 978-953-7619-50-3, InTech, Available from: http://www.intechopen.com/books/optical-fiber-new-developments/finding-hydrogen-leaks-by-means-of-the-fiber-bragg-gratings-technology

INTECH
open science | open minds

InTech Europe
University Campus STeP Ri
Slavka Krautzeka 83/A
51000 Rijeka, Croatia
Phone: +385 (51) 770 447
Fax: +385 (51) 686 166
www.intechopen.com

InTech China
Unit 405, Office Block, Hotel Equatorial Shanghai
No.65, Yan An Road (West), Shanghai, 200040, China
中国上海市延安西路65号上海国际贵都大饭店办公楼405单元
Phone: +86-21-62489820
Fax: +86-21-62489821

IntechOpen